

SCIENTIFIC REPORTS

OPEN

Unexpected observation of splitting of skyrmion phase in Zn doped Cu_2OSeO_3

H. C. Wu¹, T. Y. Wei¹, K. D. Chandrasekhar¹, T. Y. Chen¹, H. Berger² & H. D. Yang¹

Received: 28 April 2015

Accepted: 31 July 2015

Published: 09 September 2015

Polycrystalline $(\text{Cu}_{1-x}\text{Zn}_x)_2\text{OSeO}_3$ ($0 \leq x \leq 0.2$) samples were synthesized using solid-state reaction and characterized by X-ray diffraction (XRD). The effect of Zn doping upon saturation magnetization (M_s) indicates that the Zn favors to occupying Cu(II) square pyramidal crystallographic site. The AC susceptibility (χ'_{ac}) was measured at various temperatures ($\chi'_{ac}-T$) and magnetic field strengths ($\chi'_{ac}-H$). The Zn doping concentration is found to affect greatly the $M-T$ and $\chi'_{ac}-T$. The skyrmion phase has been inferred from the $\chi'_{ac}-H$ data, and then indicated within the $H-T$ phase diagrams for various Zn doping concentrations. The striking and unexpected observation is that the skyrmion phase region becomes split upon Zn doping concentration. Interestingly, second conical boundary accompanied by second skyrmion phase was also observed from $d\chi'_{ac}/dH$ vs. H curves. Atomic site disorder created by the chemical doping modulates the delicate magnetic interactions via change in the Dzyaloshinskii-Moriya (DM) vector of distorted Cu(II) square pyramidal, thereby splitting of skyrmion phase might occur. These findings illustrate the potential of using chemical and atomic modification for tuning the temperature and field dependence of skyrmion phase of Cu_2OSeO_3 .

Ever since the discovery of high- T_c superconductivity¹, copper oxide materials have garnered significant attention due to exotic physical properties such as charge order stripes², electronic phase separation³, giant magnetoresistance⁴ and multiferroics⁵. This family of materials produce complex and rich phase diagrams because of the strong interplay between their crystal lattices and the spin and orbital degrees of freedoms⁴. The prime research focus is to address the underlying mechanism behind the physical insight and to establish the technological relevance of these materials.

Recently, a peculiar magnetic state called as “skyrmion or A-phase” has been stabilized in noncentrosymmetric B20 chiral magnetic systems, such as MnSi, FeSi and FeGe^{6–8}. Magnetic skyrmion is a topologically stable particle-like spin configuration where spins mold into a vortex-like ordering. More recently, the recognition of skyrmion in insulating spin-1/2 Cu_2OSeO_3 ⁹ was reported. It has further triggered the intensive research activity because skyrmion motion can be controlled by external electric fields instead of Joule heating currents, thus making it a good candidate for ultra-low power spintronic devices^{9,10}. The skyrmion lattice can be probed with several experimental methods, such as Lorentz transmission electron microscopy¹¹, magnetic force microscopy¹², spin-polarized scanning tunneling microscopy¹³ and small angle neutron scattering¹⁴. The signature of skyrmion lattice can also be detected by relatively simple methods such as magnetic χ'_{ac} ¹⁵, heat capacity¹⁶, topological Hall effect¹⁷ and electrical polarization^{18–20}.

From the crystallographic view, the common point to both high- T_c superconductor $\text{YBa}_2\text{Cu}_3\text{O}_7$ and skyrmion Cu_2OSeO_3 systems is the presence of two different Cu sites. It indicates the microscopic picture of these novel phenomena are hidden in the local structures of two Cu ions and its complex magnetic interactions between Cu(I)/Cu(II) ions. In $\text{YBa}_2\text{Cu}_3\text{O}_7$, Cu ions are located on two different sites i.e. Cu(I)O chains and Cu(II)O₂ planes. The superconductivity mainly originates from the electron transport

¹Department of Physics, National Sun Yat-Sen University, Kaohsiung, 804 Taiwan. ²Institute of Physics of Complex Matter, Ecole Polytechnique Federal de Lausanne, CH-1015 Lausanne, Switzerland. Correspondence and requests for materials should be addressed to H.D.Y. (email: yang@mail.nsysu.edu.tw)

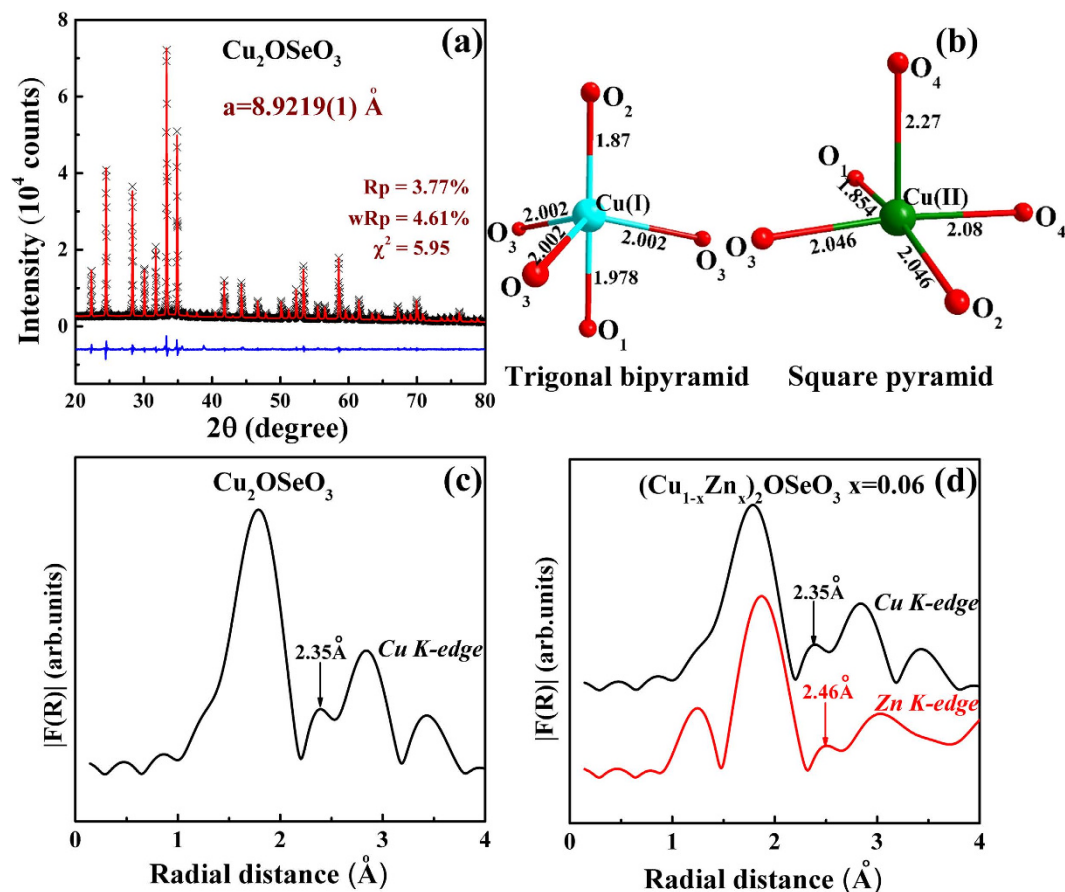


Figure 1. (a) Rietveld refinement of X-ray pattern of Cu_2OSeO_3 sample. (b) Trigonal bipyramidal and square pyramidal sites of Cu_2OSeO_3 derived from Rietveld analysis. Fourier transforms moduli radial distribution functions of EXAFS spectra (c) Cu K-edge for Cu_2OSeO_3 . (d) Cu and Zn K-edge for $(\text{Cu}_{0.94}\text{Zn}_{0.06})_2\text{OSeO}_3$ respectively. Arrows near small hump in Fig. 1 (c,d) indicate Cu(II)- O_4 and Zn- O_4 bond lengths respectively.

across the Cu(II)O_2 planes²¹. In Cu_2OSeO_3 , the two Cu^{2+} ions occupy trigonal bipyramidal (Cu(I)) and square pyramidal (Cu(II)) of oxygen ligands, with the ratio of 1:3²². Neutron scattering, μSR , and NMR experiments have established the ferrimagnetism of Cu spin with three up (Cu(II)) and one down (Cu(I)) spin alignment^{22–24}. However, a close inspection of the magnetic interactions and the crystal lattice of Cu^{2+} spins reveal the presence of more complex superexchange interactions between the Cu-O-Cu bridges^{25,26}. Interestingly, unexpected two distinct coupled skyrmion sublattices, which arise from the two different magnetic active orbitals i.e. Cu(I) and Cu(II), have been identified in Cu_2OSeO_3 system using the orbital sensitive resonant X-ray scattering²⁷. It indicates that the site-specific chemical (Cu(I)/Cu(II)) doping might help to gain further insights of this novel skyrmion phase. Following the similar study in high- T_c $\text{YBa}_2\text{Cu}_3\text{O}_7$ ²¹, we explore the chemical doping to shed the light on the microscopic origin of these two skyrmion sublattices. The primary goals of this work are to find out what is the role of Cu(I) and Cu(II) sites in the formation of skyrmion phase? What are the effects of nonmagnetic Zn doping on the skyrmion lattice? Consequently, what are the electronic and magnetic nature of skyrmion phase in Cu_2OSeO_3 ?

Results and Discussion

Figure 1(a) shows the X-ray diffraction pattern of Cu_2OSeO_3 sample. The pattern showed the cubic crystal structure and refined with P2₁3 space group using GSAS Rietveld program. The obtained lattice parameter ($a = 8.9219(1) \text{ \AA}$) consistent with the previous report indicates the good quality of the sample²². The local structures trigonal bipyramidal and square pyramidal (represented in Fig. 1(b)) determined by the Rietveld method are highly distorted similarly to previous report²². To check the Zn occupation in Cu_2OSeO_3 crystal, we have performed the room temperature extended X-ray absorption fine structure (EXAFS). EXAFS is highly sensitive technique to probe local crystal structure such as coordination number of ligand and interatomic distance of metal ion to ligand atoms²⁸. The EXAFS spectrum analysis was carried out in Athena software. The moduli of their Fourier transforms $|F(R)|$ are presented in Fig. 1(c,d). As seen from Fig. 1(c), the spectrum for Cu_2OSeO_3 at Cu K-edge shows the prominent peak around

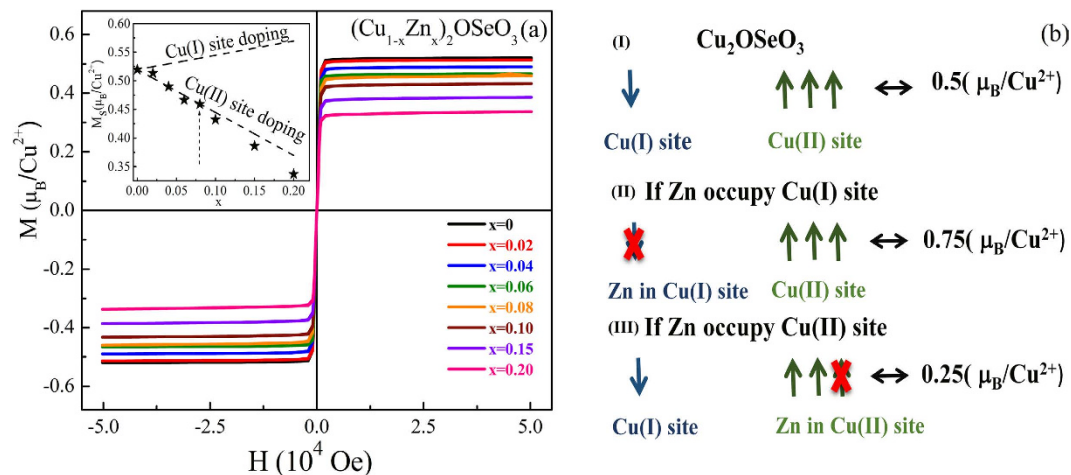


Figure 2. (a) M vs. H curves of $(\text{Cu}_{1-x}\text{Zn}_x)_2\text{OSeO}_3$ ($0 \leq x \leq 0.2$) series at $T = 5$ K; Inset shows the M_s vs. Zn doping concentration. Dashed lines indicate the theoretically predicted occupation probabilities of Zn at Cu(I) or Cu(II) crystallographic positions respectively. The experimental data matches the Cu(II) site occupation. (b) The graphical representation of resultant magnetic moment for (I) Cu_2OSeO_3 (II) Zn at Cu(I) site and (III) Zn at Cu(II) site respectively.

1.85 Å followed by the small hump at 2.35 Å. To understand the EXAFS spectrum we have compared the EXAFS spectrum with Fig. 1(b). The primary difference between these two structures of Fig. 1(b) is the axial bond length that is longer for the square pyramidal structure. By comparing EXAFS spectrum with the bond lengths of Fig. 1(b), the small hump can be assigned to the axial bond length of Cu(II)- O_4 square pyramidal. Fig. 1(d) depicts the $|F(R)|$ spectra for $(\text{Cu}_{0.94}\text{Zn}_{0.06})_2\text{OSeO}_3$ at Cu and Zn K -edges. As shown in the figure the Zn K -edge spectrum qualitatively identical to the Cu K -edge (low radial distance peak might come from other sources such as atomic XAFS and/or multielectron excitations²⁸). As expected Zn spectrum shifted to high radial distances, this indicates the enhancement of bond length due to the changes in the covalent bond formation upon Zn doping. Most importantly, Zn spectrum exhibits the Zn- O_4 bond peak even for small doping concentration (6% of Zn) which qualitatively indicates the Zn certainly occupy the Cu(II) site. On the other hand, the low Zn doping concentration hampers the quantitative estimation of Zn at Cu(II) site.

Figure 2 depicts the isothermal M - H loops at $T = 5$ K with the field up to 5 T for $(\text{Cu}_{1-x}\text{Zn}_x)_2\text{OSeO}_3$ ($0 \leq x \leq 0.2$). The saturation magnetization M_s at 5 T is observed to be $0.519 \mu_B/\text{Cu}^{2+}$ for $x = 0$, a close match with the theoretical predicted ($0.5 \mu_B/\text{Cu}^{2+}$) ferrimagnetic alignment of Cu spins⁹. For the doping case, the nonmagnetic Zn^{2+} ion might occupy two possible crystallographic (Cu(I)/Cu(II)) sites. If non-magnetic Zn replaces any one of three ferromagnetically aligned Cu(II) sites that decrease the overall magnetization of the unit cell ($0.25 \mu_B/\text{Cu}^{2+}$). On the other hand, Zn placed at Cu(I) site enhances the overall magnetization as well as ferromagnetic strength ($0.75 \mu_B/\text{Cu}^{2+}$). To estimate the probable Zn site occupation we have simulated the M_s values for both the case of Cu(I)/Cu(II) sites. The inset also plots the theoretically predicted values that would be expected for each of doping sites. The measured values line up well with theoretical expectation for the Cu(II) sites, which reveals that the nonmagnetic Zn^{2+} ions favor occupying the Cu(II) site.

Figure 3 shows the M - T and χ'_{ac} - T curves for $(\text{Cu}_{1-x}\text{Zn}_x)_2\text{OSeO}_3$ ($0 \leq x \leq 0.2$). For $x = 0$, the M - T and χ'_{ac} - T curves are in good agreement with those of measured in single crystal Cu_2OSeO_3 ²⁹. Moreover, both M - T and χ'_{ac} - T are changed correspondingly and systematically with Zn doping concentration x . Just below ferrimagnetic transition $T_C \sim 58$ K, a clear peak appeared at 56 K shown in χ'_{ac} - T for $x = 0$ is the hallmark signature of skyrmion phase³⁰. It is noted that the peak is lowered in temperature and becomes fainter with increasing x . On the other hand, a second smaller but notable peak is developed as $x \geq 0.02$ and shifted towards lower temperature with increasing x . These results clearly hint the possible formation of second skyrmion phase when $x \geq 0.02$.

AC susceptibility is known to be a sensitive technique for revealing coexisting phases in complex magnetic materials, including skyrmion system^{15,25}. The H dependent χ'_{ac} curves at 50–58 K are shown in Fig. 4(a) for Cu_2OSeO_3 . Below the vicinity of peak temperature ~ 56 K as shown Fig. 3b, the evolution of peak anomalies is noticed in the intermediate field region $100 \leq H \leq 400$ Oe in χ'_{ac} vs. H curves (Fig. 4(a)). It confirms the growth of skyrmion phase^{15,25} as $T \leq 56$ K. For low temperatures, the peak anomalies suppress in the χ'_{ac} vs. H curves which indicates the skyrmion phase is almost disappeared for $T < 52$ K. To demonstrate the typical way of extracting the skyrmion phase boundaries, the χ'_{ac} vs. H curves at selected temperatures $T_1 = 57$ K, $T_2 = 56$ K, $T_3 = 55$ K, $T_4 = 53$ K and $T_5 = 51$ K are shown in Fig. 4(b). The H - T phase diagram with skyrmion zone marked in red for Cu_2OSeO_3 is successfully

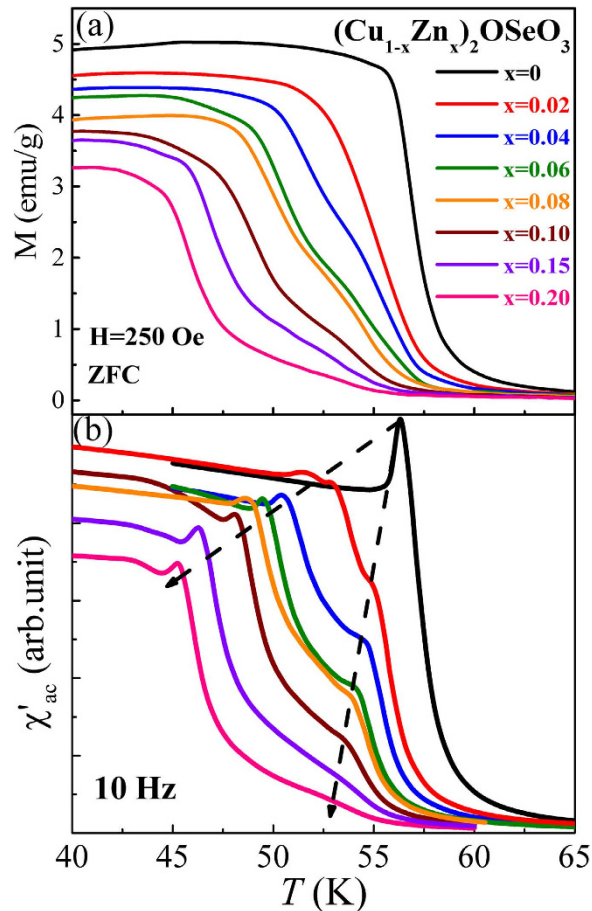


Figure 3. (a) M vs. T (b) χ'_{ac} vs. T curves for $(\text{Cu}_{1-x}\text{Zn}_x)_2\text{OSeO}_3$ ($0 \leq x \leq 0.2$). The dashed lines in (b) added as a guide to the eye for variation of magnetic transition temperatures with Zn doping.

constructed and displayed in Fig. 4(c). The evolution of different magnetic phase zones, i.e. helical, conical and skyrmion boundaries are in good agreement with previously published results¹⁴.

To investigate the influence of Zn doping on the skyrmion phase of Cu_2OSeO_3 , the χ'_{ac} vs. H for $(\text{Cu}_{1-x}\text{Zn}_x)_2\text{OSeO}_3$ ($0 \leq x \leq 0.2$) are performed for a broad range of T . The representative results of $x = 0.1$ are shown in the Fig. 5(a). The characteristic features of the χ'_{ac} vs. H curves for $x = 0.1$ at $51 \text{ K} \leq T \leq 53 \text{ K}$ are comparable to that of Cu_2OSeO_3 at $52 \text{ K} \leq T \leq 56 \text{ K}$ (shown in Fig. 4(a)), that the signature of skyrmion phase is noticed with two peaks. With decreasing temperature to $48 \text{ K} < T < 51 \text{ K}$, the two peaks become smeared. However, as the temperature is lowered to $47 \text{ K} \leq T \leq 48 \text{ K}$, the signature of skyrmion peaks reappeared for H between 80 and 210 Oe. This unexpected observation of second skyrmion phase is a quite novel phenomenon and never been reported in the Cu_2OSeO_3 system. Along with second skyrmion signature, χ'_{ac} displays second inflection point in the $d\chi'_{ac}/dH$ vs. H (see supplementary material) curves. It might indicate the appearance of the second conical boundary in the phase diagram accompanied with the second skyrmion phase. However, further experimental verification needed to confirm these signatures. It is important to emphasize that, similar atomic doping effect in a metallic skyrmion systems such as $\text{Mn}_{1-x}\text{Fe}_x\text{Si}$ and $\text{Mn}_{1-x}\text{Co}_x\text{Si}$ ³¹ lead to Quantum phase transitions with a suppressed of helical magnetic and skyrmion phases. Contradictory, the present study indicates the atomic disorder strongly influence the ground state magnetic properties of the Cu_2OSeO_3 system that lead to more complex magnetic behavior with the generation of additional novel phases in the H - T phase diagram. The multiple inflection points in $d\chi'_{ac}/dH$ vs. H curves are systematically changes with the Zn doping concentration in a selected temperature window, which are displayed in the supplementary material. Following the same plotting procedure as mentioned in Fig. 4(b,c), the Fig. 5(b) is successfully constructed from Fig. 5(a).

Applying the same method as described in Figs 4 and 5, the H - T phase diagrams derived from χ'_{ac} - H data at selected temperatures for each of 8 samples $(\text{Cu}_{1-x}\text{Zn}_x)_2\text{OSeO}_3$ ($0 \leq x \leq 0.2$) are established and shown in Fig. 6, where the boundaries of conical, helical and skyrmion phases are plotted (with various colors) approximately using limited and discrete data points. The surprising finding is that the single skyrmion phase at $x = 0$ is splitted into two well-defined small branches in two different temperature regions and about the same magnetic field as $x \geq 0.02$. Moreover, the second skyrmion phase is hosted by

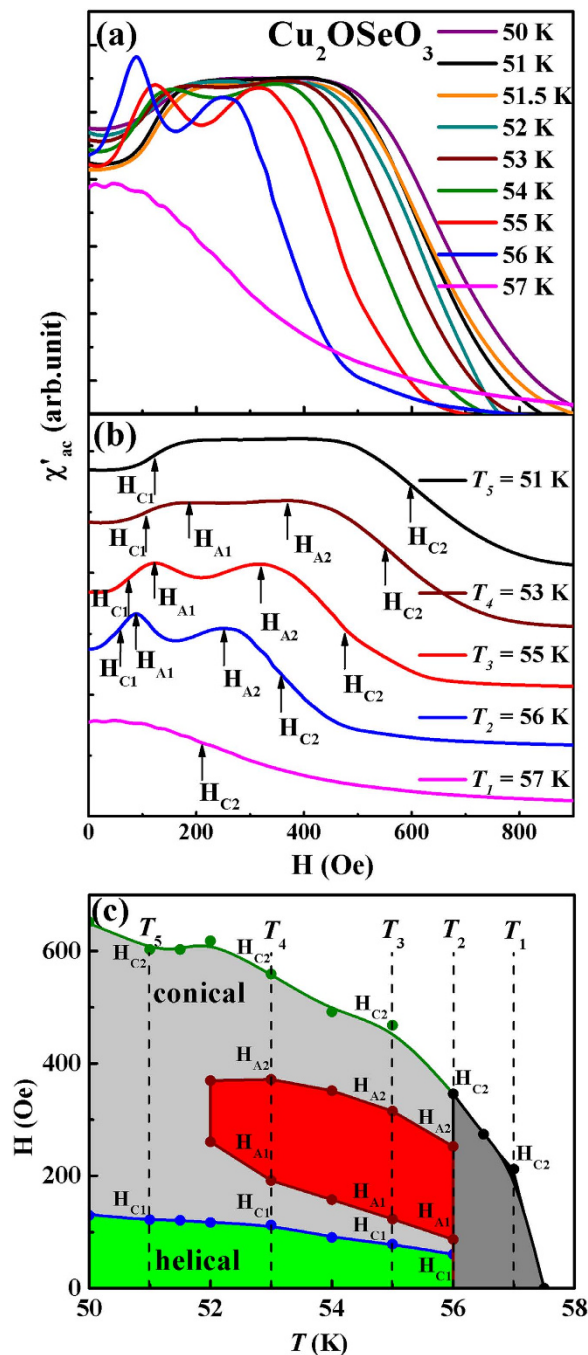


Figure 4. (a) χ'_{ac} vs. H plot at temperatures 50–57 K. (b) Selected temperature curves from (a), but offset each other for easy comparison. The notations of H_{A1} and H_{A2} indicate skyrmion phase boundaries while H_{C1} and H_{C2} indicate conical phase boundaries respectively. The values of H_{A1} and H_{A2} are determined by the peaks while H_{C1} and H_{C2} are the inflection points in the first derivative of χ'_{ac} vs. H curves. (c) H vs. T phase diagram for Cu_2OSeO_3 , where the skyrmion phase zone is marked in red.

the second conical phase boundary. Both branches of skyrmion phase are systematically shifted towards low temperature side with x . The opening of temperature gap between two branches of skyrmion phase is larger for higher Zn doping concentration. The second skyrmion phase and its associated conical phase boundaries are firmly decoupled with that of the initial skyrmion phase; this can be clearly visible for the doping concentration $x \geq 0.1$. Meanwhile, the high-temperature branch becomes harder to extract from the data as $x > 0.15$. In fact, the trends of splitting, suppression, and decreasing in temperature of skyrmion phases found in Fig. 6 are consistent with those observed in Fig. 3(b).

The splitting of skyrmion phase for Zn doping Cu_2OSeO_3 is a novel and interesting phenomenon. Similar to high- T_c superconducting materials, it might be associated with the two crystallographic sites of

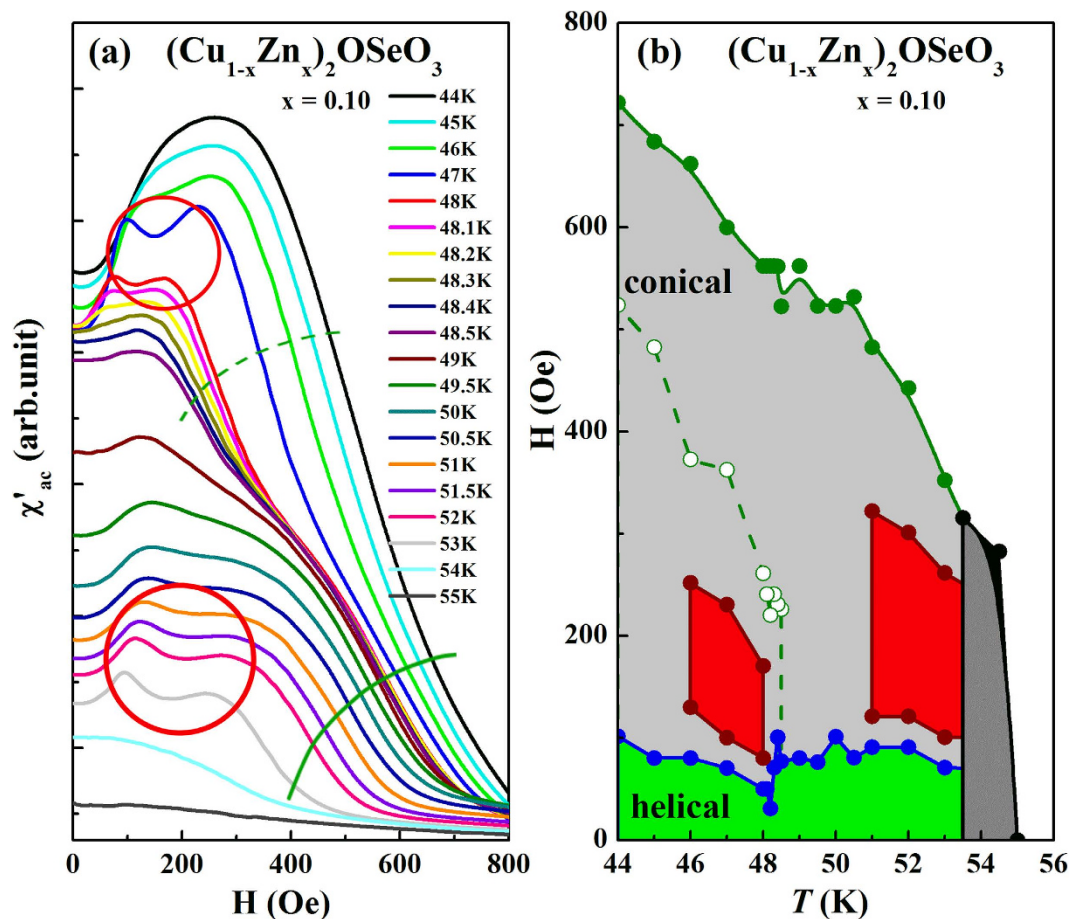


Figure 5. (a) χ'_{ac} vs. H of at temperatures 44–55 K and (b) corresponding H vs. T phase diagram for $(\text{Cu}_{1-x}\text{Zn}_x)_2\text{OSeO}_3$ ($x=0.1$). The two red circles in (a) corresponding to respective skyrmion zones in (b). Solid and dashed green lines denote the conical phase boundaries.

Cu ions and their complex magnetic interactions. From the magnetic point of view, Cu_2OSeO_3 exhibits a quite complex behavior with several magnetic interactions between Cu(I)/Cu(II) via oxygen bridging²⁵. In the unit cell of Cu_2OSeO_3 structure, the 4 Cu(I) ions are placed in the undistorted trigonal bipyramidal, whereas 12 Cu(II) ions are distributed among the distorted square pyramidal sites. According to Goodenough-Kramer (G-K) rules, a negative superexchange interaction ($<J$) corresponds to the orbital overlap angle of Cu ions close to 90° , and it goes to positive ($>J$) if it deviates from 90° ³². A close examination of Cu_2OSeO_3 using an AC susceptibility technique exposed the antiferromagnetic (AFM) ordering at 59 K followed by ferromagnetic (FM) ordering at 58 K²⁵. The complicated behaviour originates from the unequal strength of three nearest neighbors (NN) AFM interaction of Cu(I)-Cu(II) and three NN FM interaction of Cu(II)-Cu(II) ions²⁵. The crystallography studies in Fig. 1 along with magnetization studies in Fig. 2 suggest that the Cu(II) is the preferable site for Zn doping. Replacing of nonmagnetic Zn^{2+} for Cu^{2+} site enhances the Coulombic repulsion of electronic orbital that leads to the decrease in T_C . Moreover, the presence of nonmagnetic dopant along with the weak perturbation for the overlaps of electronic orbital can show a significant impact on the complex magnetic exchange interactions between Cu(I)/Cu(II) ions. In general, the helical ground state originates from the competition between Heisenberg superexchange and DM interactions of Cu ions⁹. The strength of DM interaction depends on the relative change of g -factor from the free electron g -value, i.e. $\text{DM} \propto (\Delta g/g)J$, where J is the exchange interaction term³³. Symmetry calculation analysis using Raman modes by Gnezdilov *et al.* indicates the change of DM strength is more significant for the distorted Cu(II) square pyramidal³³. The disorder effect is further amplified by doping the nonmagnetic Zn that strongly modulates the DM interaction strength via the change of radial vector and the canting angle between the adjacent spin pairs. Consequently, it manipulates the complex magnetic interactions between Cu(I)/Cu(II) ions.

Similar to resonant X-ray scattering studies on Cu_2OSeO_3 , these two skyrmion phases can be possibly associated with the two Cu sublattices²⁷. Chemical doping might alter the modulation vector of Moirelike skyrmion phase of pure Cu_2OSeO_3 . These results reminiscent the recent observation of unexpected coupled skyrmion sublattices²⁷ and theoretical prediction of novel half skyrmion state in Cu_2OSeO_3 system³⁴. However, it needs more experimental verifications whether the second skyrmion

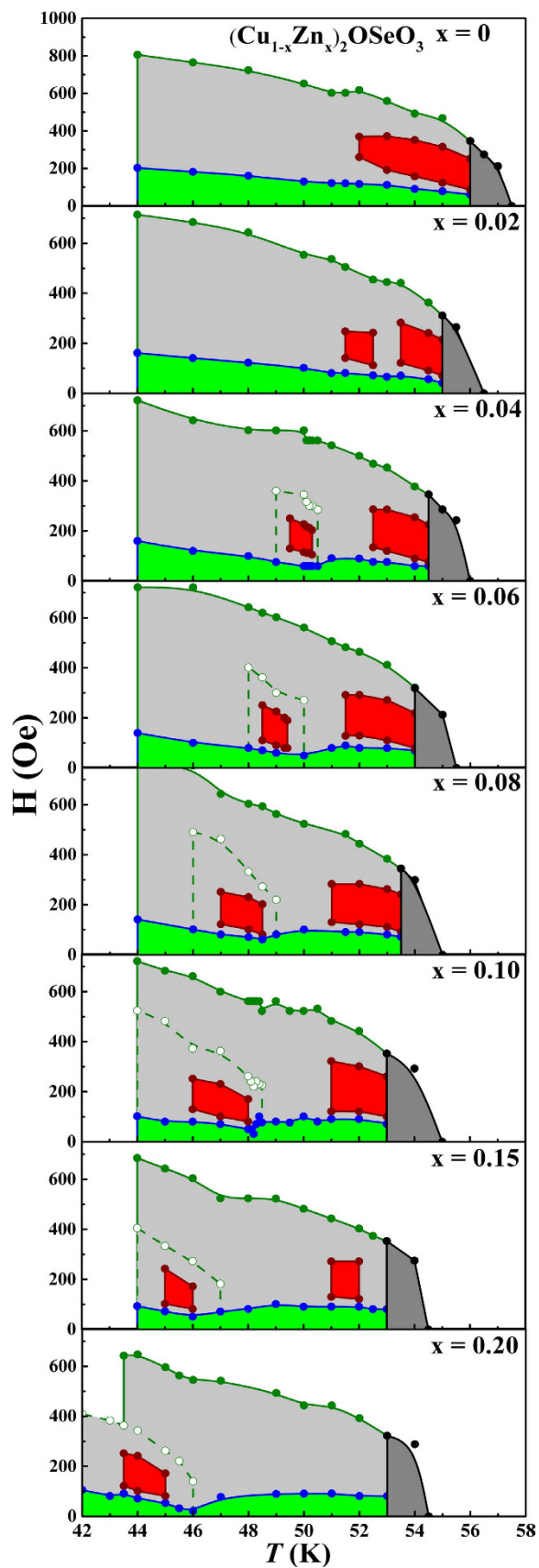


Figure 6. H-T phase diagrams of all $(\text{Cu}_{1-x}\text{Zn}_x)_2\text{OSeO}_3$ ($0 \leq x \leq 0.2$) samples. Skyrmion zone is indicated by two red areas respectively. Solid and dashed green lines denote the two conical phase boundaries respectively.

and its accompanied conical phase are originated from decoupling of coupled Cu skyrmion sublattices or it is related to new kind of spin skyrmion structure. A detailed reciprocal space map using the neutron scattering and scanning tunneling microscope studies are particularly required to shed light on this complex skyrmion behavior. Our findings open up a new pathway for further experimental and theoretical research to elucidate the exotic quantum topological skyrmion phases using chemical doping.

In summary, we have successfully synthesized and well characterized the high quality polycrystalline $(\text{Cu}_{1-x}\text{Zn}_x)_2\text{OSeO}_3$ ($0 \leq x \leq 0.2$) samples. Zn doped skyrmion exhibits the complex and rich phase diagram. The significant findings are: (1) The dopant Zn is favored to occupy the Cu(II) square pyramid crystallographic site. (2) The M - T and χ'_{ac} - T are changed dramatically with the increase of Zn doping concentration. (3) The skyrmion phase shown in H - T phase diagram of Cu_2OSeO_3 is split with Zn doping as demonstrated in detailed H and T dependent χ'_{ac} data. (4) Second conical boundary extracted from the $d\chi'_{ac}/dH$ vs. H curves accompanied by the second skyrmion phase. All these results suggest a interesting novel scenario and this unexpected observed appearance of second skyrmion and its conical boundary might be related to the way that the Zn doping manipulates the DM vector of the distorted Cu(II)O₅ square pyramid through the influence of delicate magnetic interactions. These results point to a new direction of tuning the skyrmion lattice in Cu_2OSeO_3 by assorted chemical and atomic modification.

Methods

In this study, polycrystalline samples of $(\text{Cu}_{1-x}\text{Zn}_x)_2\text{OSeO}_3$ ($0 \leq x \leq 0.2$) were prepared by solid-state reaction method. Nominal mixtures of high purity CuO, ZnO, and SeO₂ powders were pressed into pellets. The pellets were sealed in an evacuated quartz tube and heated to a temperature range of 520 °C to 600 °C for 72 h, then slowly cooled over several hours to room temperature. This process was repeated at least twice with intermediate grinding. X-ray diffraction patterns show good quality of samples, with only a minor impurity phases appearing when $x \geq 0.06$. Homogeneity of Zn distribution was analyzed with energy dispersive X-ray analysis, which indicated a uniform distribution of Zn throughout the sample (the supplementary material). Temperature and field dependent DC magnetization and AC susceptibility measurements were performed by a SQUID magnetometer (MPMS-XL7, Quantum Design). EXAFS K -edge experiments were carried out in transmission mode for Cu and fluorescence mode for Zn respectively at the 17C beamline in the National Synchrotron Radiation Research Center (NSRRC), Hsinchu, Taiwan.

References

1. Wu, M. K. *et al.* Superconductivity at 93 K in a new mixed-phase Y-Ba-Cu-O compound system at ambient pressure. *Phys. Rev. Lett.* **58**, 908–910 (1987).
2. Mook, H. A., Dai, P. & Doğan, F. Charge and Spin Structure in $\text{YBa}_2\text{Cu}_3\text{O}_{6.35}$. *Phys. Rev. Lett.* **88**, 097004 (2002).
3. Matsuda, M. *et al.* Electronic phase separation in lightly doped $\text{La}_{2-x}\text{Sr}_x\text{CuO}_4$. *Phys. Rev. B* **65**, 134515 (2002).
4. Kastner, M. A., Birgeneau, R. J., Shirane, G. & Endoh, Y. Magnetic, transport, and optical properties of monolayer copper oxides. *Rev. Mod. Phys.* **70**, 897–928 (1998).
5. Kimura, T., Sekio, Y., Nakamura, H., Siegrist, T. & Ramirez, A. P. Cupric oxide as an induced-multiferroic with high- T_C . *Nat. Mater.* **7**, 291–294 (2008).
6. Mühlbauer, S. *et al.* Skyrmion Lattice in a Chiral Magnet. *Science* **323**, 915–919 (2009).
7. Nagaosa, N. & Tokura, Y. Topological properties and dynamics of magnetic skyrmions. *Nat. Nanotech* **8**, 899–911 (2013).
8. Huang, S. X. & Chien, C. L. Extended Skyrmion Phase in Epitaxial $\text{FeGe}(111)$ Thin Films. *Phys. Rev. Lett.* **108**, 267201 (2012).
9. Seki, S., Yu, X. Z., Ishiwata, S. & Tokura, Y. Observation of Skyrmions in a Multiferroic Material. *Science* **336**, 198–201 (2012).
10. Felsner, C. Skyrmions. *Angew. Chem. Int. Ed.* **52**, 1631–1634 (2013).
11. Yu, X. Z. *et al.* Real-space observation of a two-dimensional skyrmion crystal. *Nature* **465**, 901–904 (2010).
12. Milde, P. *et al.* Unwinding of a Skyrmion Lattice by Magnetic Monopoles. *Science* **340**, 1076–1080 (2013).
13. Kirsten von, B., André, K., Oswald, P. & Roland, W. Interface-induced chiral domain walls, spin spirals and skyrmions revealed by spin-polarized scanning tunneling microscopy. *J. Phys.: Condens. Matter* **26**, 394002 (2014).
14. Adams, T. *et al.* Long-Wavelength Helimagnetic Order and Skyrmion Lattice Phase in Cu_2OSeO_3 . *Phys. Rev. Lett.* **108**, 237204 (2012).
15. Bauer, A. & Pfleiderer, C. Magnetic phase diagram of MnSi inferred from magnetization and ac susceptibility. *Phys. Rev. B* **85**, 214418 (2012).
16. Bauer, A., Garst, M. & Pfleiderer, C. Specific Heat of the Skyrmion Lattice Phase and Field-Induced Tricritical Point in MnSi. *Phys. Rev. Lett.* **110**, 177207 (2013).
17. Neubauer, A. *et al.* Topological Hall Effect in the A Phase of MnSi. *Phys. Rev. Lett.* **102**, 186602 (2009).
18. Belesi, M. *et al.* Magnetoelectric effects in single crystals of the cubic ferrimagnetic helimagnet Cu_2OSeO_3 . *Phys. Rev. B* **85**, 224413 (2012).
19. Omrani, A. A. *et al.* Exploration of the helimagnetic and skyrmion lattice phase diagram in Cu_2OSeO_3 using magnetoelectric susceptibility. *Phys. Rev. B* **89**, 064406 (2014).
20. Chu, P. *et al.* Real-space anisotropic dielectric response in a multiferroic skyrmion lattice. *Sci. Rep.* **5**, 8318 (2015).
21. Xiao, G. *et al.* High-temperature superconductivity in tetragonal perovskite structures: Is oxygen-vacancy order important? *Phys. Rev. Lett.* **60**, 1446–1449 (1988).
22. Bos, J.-W. G., Colin, C. V. & Palstra, T. T. M. Magnetoelectric coupling in the cubic ferrimagnet Cu_2OSeO_3 . *Phys. Rev. B* **78**, 094416 (2008).
23. Maisuradze, A. *et al.* μSR investigation of magnetism and magnetoelectric coupling in Cu_2OSeO_3 . *Phys. Rev. B* **84**, 064433 (2011).
24. Belesi, M. *et al.* Ferrimagnetism of the magnetoelectric compound Cu_2OSeO_3 probed by ^{77}Se NMR. *Phys. Rev. B* **82**, 094422 (2010).
25. Živković, I., Pajić, D., Ivek, T. & Berger, H. Two-step transition in a magnetoelectric ferrimagnet Cu_2OSeO_3 . *Phys. Rev. B* **85**, 224402 (2012).
26. Yang, J. H. *et al.* Strong Dzyaloshinskii-Moriya Interaction and Origin of Ferroelectricity in Cu_2OSeO_3 . *Phys. Rev. Lett.* **109**, 107203 (2012).

27. Langner, M. C. *et al.* Coupled Skyrmion Sublattices in Cu_2OSeO_3 . *Phys. Rev. Lett.* **112**, 167202 (2014).
28. Teo, B. K. *EXAFS: basic principles and data analysis.* (Springer-Verlag, 1986).
29. Huang, C. L. *et al.* Observation of a second metastable spin-ordered state in ferrimagnet Cu_2OSeO_3 . *Phys. Rev. B* **83**, 052402 (2011).
30. Zivkovic, I., White, J. S., Ronnow, H. M., Prsa, K. & Berger, H. Critical scaling in the cubic helimagnet Cu_2OSeO_3 . *Phys. Rev. B* **89**, 060401(R) (2014).
31. Bauer, A. *et al.* Quantum phase transitions in single-crystal $\text{Mn}_{1-x}\text{Fe}_x\text{Si}$ and $\text{Mn}_{1-x}\text{Co}_x\text{Si}$: Crystal growth, magnetization, ac susceptibility, and specific heat. *Phys. Rev. B* **82**, 064404 (2010).
32. Goodenough, J. B. *Magnetism and the chemical bond.* (Interscience Publishers, 1963).
33. Gnezdilov, V. P. *et al.* Magnetoelectricity in the ferrimagnetic Cu_2OSeO_3 : symmetry analysis and Raman scattering study. *Low Temp. Phys.* **36**, 550–557 (2010).
34. Janson, O. *et al.* The quantum nature of skyrmions and half-skyrmions in Cu_2OSeO_3 . *Nature Communications* **5**, 5376 (2014).

Acknowledgments

This work was supported by the Ministry of Science and Technology, Taiwan, under Grant No. MOST: 103-2112-M-110-010-MY3.

Author Contributions

H.D.Y. supervised the project. K.D.C. and H.C.W. have equal contribution to this work for the characterization and analysis of the experimental data. H.D.Y. and H.B. initiated the original idea. T.Y.W. and T.Y.C. involved in sample synthesis and characterization. K.D.C., H.D.Y. and H.C.W. wrote the manuscript.

Additional Information

Supplementary information accompanies this paper at <http://www.nature.com/srep>

Competing financial interests: The authors declare no competing financial interests.

How to cite this article: Wu, H. C. *et al.* Unexpected observation of splitting of skyrmion phase in Zn doped Cu_2OSeO_3 . *Sci. Rep.* **5**, 13579; doi: 10.1038/srep13579 (2015).



This work is licensed under a Creative Commons Attribution 4.0 International License. The images or other third party material in this article are included in the article's Creative Commons license, unless indicated otherwise in the credit line; if the material is not included under the Creative Commons license, users will need to obtain permission from the license holder to reproduce the material. To view a copy of this license, visit <http://creativecommons.org/licenses/by/4.0/>